

Serveur Académique Lausannois SERVAL serval.unil.ch

Author Manuscript

Faculty of Biology and Medicine Publication

This paper has been peer-reviewed but does not include the final publisher proof-corrections or journal pagination.

Published in final edited form as:

Title: Glutathione deficit impairs myelin maturation: relevance for white matter integrity in schizophrenia patients.

Authors: Monin A, Baumann PS, Griffa A, Xin L, Mekle R, Fournier M, Butticaz C, Klaey M, Cabungcal JH, Steullet P, Ferrari C, Cuenod M, Gruetter R, Thiran JP, Hagmann P, Conus P, Do KQ

Journal: Molecular psychiatry

Year: 2015 Jul

Issue: 20

Volume: 7

Pages: 827-38

DOI: [10.1038/mp.2014.88](https://doi.org/10.1038/mp.2014.88)

In the absence of a copyright statement, users should assume that standard copyright protection applies, unless the article contains an explicit statement to the contrary. In case of doubt, contact the journal publisher to verify the copyright status of an article.

Glutathione deficit impairs myelin maturation in experimental models: relevance for white matter integrity in schizophrenia patients

Authors

Aline Monin^{1,3}, Philipp S. Baumann^{1,2,3}, Alessandra Griffa^{4,7}, Lijing Xin⁵, Ralf Mekle⁶, Margot Fournier^{1,3}, Christophe Buttica^{1,3}, Magali Klaey^{1,3}, Jan-Harry Cabungcal^{1,3}, Pascal Steullet^{1,3}, Carina Ferrari^{1,3}, Michel Cuenod^{1,3}, Rolf Gruetter^{5,7}, Jean-Philippe Thiran^{4,7}, Patric Hagmann^{4,7}, Philippe Conus^{2,3}, Kim Q. Do^{1,3}

Affiliations

¹Center for Psychiatric Neuroscience, ²Service of General Psychiatry and ³Department of Psychiatry, Centre Hospitalier Universitaire Vaudois and University of Lausanne (CHUV-UNIL), Lausanne, Switzerland

⁴Signal Processing Laboratory, Ecole Polytechnique Fédérale de Lausanne (EPFL), Lausanne, Switzerland

⁵Laboratory for Functional and Metabolic Imaging, Ecole Polytechnique Fédérale de Lausanne (EPFL), Lausanne, Switzerland

⁶Physikalisch-Technische Bundesanstalt, Berlin, Germany

⁷Department of Radiology, Centre Hospitalier Universitaire Vaudois and University of Lausanne (CHUV-UNIL), Lausanne, Switzerland

Correspondence

Professor Kim Q. Do
Department of Psychiatry
Center for Psychiatric Neuroscience
Centre Hospitalier Universitaire Vaudois and University of Lausanne
1008 Prilly-Lausanne, Switzerland
E-mail: kim.do@chuv.ch

Abstract

Schizophrenia pathophysiology implies both redox dysregulation and dysconnectivity of prefrontal cortex, likely related to oligodendrocyte and myelin impairments. As oligodendrocytes are highly vulnerable to oxidative stress, we investigated the interplay between glutathione and myelin. In control subjects, multimodal brain imaging revealed a positive association between medial prefrontal glutathione levels and both white matter integrity and resting-state functional connectivity along the cingulum bundle. In early psychosis patients, only white matter integrity was correlated with glutathione levels. On the other side, in prefrontal cortex of peripubertal mice with genetically impaired glutathione synthesis, mature oligodendrocyte numbers, as well as myelin markers were decreased. At the molecular levels, under glutathione deficit conditions induced by shRNA targeting the key glutathione synthesis enzyme, oligodendrocyte progenitors showed a decreased proliferation mediated by an upregulation of Fyn kinase activity, reversed by either the antioxidant N-acetylcysteine or Fyn kinase inhibitors. In addition, oligodendrocyte maturation was impaired. Interestingly, the regulation of Fyn mRNA and protein expression was also impaired in fibroblasts of patients deficient in glutathione synthesis. Thus, glutathione and redox regulation play a critical role in myelination processes and white matter maturation in prefrontal cortex of rodent and human, a mechanism potentially disrupted in schizophrenia.

Keywords: schizophrenia; glutathione; myelin; Fyn; MRI; oxidative stress

Introduction

Abnormalities in brain connectivity appear to be cardinal features of schizophrenia, and recent research has focused on white matter and factors affecting its integrity (1). Findings from transcriptomics (1-3), neuropathology (4-6) and neuroimaging (1, 7-9) provide compelling evidence for alterations of oligodendrocytes and myelin in various subregions of the prefrontal cortex including anterior cingulate cortex of schizophrenia patients. Nevertheless, the underlying pathophysiological mechanisms are still elusive and their clarification would require investigating the early phase of the disease as their developmental emergence would be masked by chronicity.

Converging data indicate a role for redox dysregulation in the pathophysiology of schizophrenia (10-13). In some studies, decreased glutathione (GSH) levels, the main cellular non-protein antioxidant and redox regulator (14, 15), have been reported in cerebrospinal fluid and prefrontal cortex of patients by using Magnetic Resonance Spectroscopy (MRS) (16, 17) and in *postmortem* tissues (13, 18). Moreover, the abnormal function of proteins encoded by various candidate genes for schizophrenias (i.e. *PRODH* (19), *DISC1* (20), *G72* (21), *DTNBPI* (22), *NRG1* (23)) can increase the production of reactive oxygen species (ROS) and therefore induce oxidative stress (19, 21, 24-26). We have thus proposed that developmental redox dysregulation constitutes one final common pathway, on which converge genetic and environmental vulnerability factors generating oxidative stress (11). In addition, polymorphisms in the genes coding for the catalytic (*GCLC*) (27) and modifier (*GCLM*) (28) subunits of the glutamate-cysteine ligase (GCL), the rate-limiting enzyme for GSH synthesis, are associated with schizophrenia in case-control studies. The GAG trinucleotide repeat polymorphisms of *GCLC*, which are more frequent in patients (“GAG high-risk” genotypes) (27), are associated with changes in plasma thiol levels (29). Compared to the “GAG low-risk” genotypes, GCL activity and GSH content in fibroblasts are lower in “GAG high-risk”

genotypes under oxidative stress conditions (27). These data prompted the investigation of *GCLM* knockout mice (*GCLM*-KO) as a model of schizophrenia. In developing and adult animals, brain GSH levels are decreased by 70% (30), and *GCLM*-KO mice show signs of oxidative stress in discrete brain regions (30, 31), including the anterior cingulate cortex (31). These mice present behavioral alterations such as impaired sensory gating, abnormal response to environmental novelty, abnormal social and emotion-related behaviors (32), all known as hallmarks of the disease.

In fact, oligodendrocytes are highly vulnerable to oxidative stress. They display high metabolic activity and contain large stores of iron (33), both of which favor ROS production. Despite of that, they contain three times less GSH than astrocytes (33). Oligodendrocytes and their progenitors are particularly sensitive to hydrogen peroxide (15) and nitric oxide inducers (34). Moreover, a GSH deficit decreases the survival of oligodendrocyte progenitor cells (OPC) *in vitro* (35).

The notion that a redox dysregulation during critical periods of neurodevelopment could alter structural and functional connectivity has not yet been established. We propose that redox dysregulation and oxidative stress could contribute to the white matter anomalies observed in schizophrenia. We thus hypothesized that GSH levels in the medial prefrontal cortex can be involved in the white matter integrity of the cingulum bundle, a fiber tract connecting frontal brain areas to posterior limbic structures. The finding of an association between prefrontal GSH levels and the cingulum white matter integrity in humans motivated us to study further the underlying mechanisms in experimental models. The consequences of a GSH deficit on OPC and myelination during development were characterized using *in vitro* and *in vivo* models, including *GCLM*-KO mice.

Materials and Methods

Subject recruitment

Patients in the early phase of psychosis, having met the threshold for psychosis (according to the CAARMS criteria) (36) were recruited from the TIPP Program (Treatment and Early Intervention in Psychosis Program, University Hospital, Lausanne, Switzerland) (37). Normal controls were recruited and assessed by the Diagnostic Interview for Genetic Studies (38). Major mood, psychotic, or substance-use disorder and having a first-degree relative with a psychotic disorder were exclusion criteria for controls. At the time of the MRI study, 28 patients were receiving antipsychotic medication. Eleven patients were receiving quetiapine, 7 aripiprazole, 4 olanzapine, 3 amisulpride, 2 risperidone and 1 paliperidone. At the time of Fyn study, 24 patients were receiving antipsychotic medication. Five patients were receiving quetiapine, 4 aripiprazole, 6 olanzapine, 3 amisulpride, 5 risperidone and 1 clozapine (see Table 1a-c for details on demographic information and chlorpromazine equivalents). Statistical analysis with one-way ANOVA did not reveal any significant effect of chlorpromazine equivalents of antipsychotic drugs on GSH, Fyn mRNA and Fyn protein expression.

Diffusion and functional MRI acquisition and data processing

MRI was performed for all subjects on a 3 Tesla scanner (Trio, Siemens Medical, Germany) with a 32-channel head-coil. Diffusion Spectrum Imaging (DSI) was acquired and reconstructed as described in Wedeen *et al.* (39). Specifically, diffusion weighted images were sampled in a Cartesian 3D grid of q-space using 128 diffusion encoding gradients covering a hemisphere with b-values varying between 0 and 8000 s/mm². The acquisition volume was made of 96x96x34 voxels of 2.2x2.2x3 mm³; TR/TE were respectively 6100/144 ms. Acquisition time was approximately 13 min. In addition, each subject was scanned in

resting state conditions using a standard gradient echo EPI sequence sensitive to BOLD contrast. An axial plane was used with a matrix of 64x58 voxels, each 3.3x3.3 mm. Thirty-two slices of 3.3 mm thickness with a 0.3 mm gap were acquired. Repetition time was 1920 ms, and acquisition time was 9 min.

Furthermore, a magnetization-prepared rapid acquisition gradient echo (MPRAGE) sequence was acquired in a matrix of 240x256x160 voxels, 1 mm in-plane resolution and 1.2 mm slice thickness. TR/TI/TE were respectively 2300/900/2.98 ms. Acquisition time was approximately 4 min.

DSI, resting state fMRI and MPRAGE data were processed using the Connectome Mapping Toolkit (www.cmtk.org) (40) and the Connectivity Decoding Toolkit (41), as described below.

gFA in the cingulum bundle: (1) Gray and white matter were segmented from the MPRAGE acquisition, and the cortical surface was partitioned into 68 regions of interest (ROIs) with FreeSurfer software (<http://surfer.nmr.mgh.harvard.edu/>) according to the Desikan-Killiany atlas (42). (2) Whole-brain streamline tractography was performed from the DSI using in-house software (37). (3) Average gFA was extracted along the cingulum bundle defined as the connections between FreeSurfer regions: medial orbitofrontal, rostral anterior cingulate, caudal anterior cingulate, posterior cingulate, isthmus of cingulate, and precuneus (43) (Figure 1a).

Functional connectivity along the cingulum bundle: (1) fMRI volumes were preprocessed including motion correction, regression of movement, average white matter and cerebrospinal fluid signals, and linear detrending. (2) Resting state time series were averaged over the FreeSurfer cortical ROIs, and band-pass filtered using the discrete wavelet transform (41). (3)

Functional correlation through the cingulum bundle was characterized with the Pearson correlation between the average low frequency cortical signals extracted from the medial prefrontal cortex (covering medial orbitofrontal and superior frontal cortex) on the one hand, and isthmus of the cingulate cortex and precuneus on the other hand (Figure 1a).

MRS and data processing

All MRS experiments were performed with a transverse electromagnetic (TEM) volume head coil (MR Instruments, Inc., Minneapolis, MN, USA). The magnetic field homogeneity was optimized by adjusting first- and second-order shims using FAST(EST)MAP (44). In vivo ^1H NMR spectra were acquired from a volume of interest (VOI) positioned in the medial bilateral prefrontal lobe using short-TE spin-echo full-intensity acquired localized single voxel spectroscopy technique (45, 46). The following scan parameters were used: VOI=20x20x25mm³, TR/TE=4000/6ms, acquisition bandwidth=2kHz, number of averaged=148, vector size=2048. GSH concentration was obtained by analyzing water suppressed in vivo ^1H NMR spectra using LCModel (47) with a basis set consisting of simulated individual metabolite spectra (48). Unsuppressed water ^1H NMR spectra were used as an internal reference for the quantification of metabolite concentrations. The spectral range for analysis was set to 0.2-4.2 ppm. By using the short-TE MRS technique at 3T, GSH was quantified with a Cramer-Rao lower bounds of $7 \pm 2\%$ (mean \pm s.d.).

Fibroblast cell culture and treatment

Fibroblast cell cultures were obtained from skin biopsies using a standard procedure (28). Cells were grown in Dulbecco's Modified Eagle's Medium (DMEM) supplemented with 2% Ultrosor-G serum (Bioprepa), 1 mM sodium pyruvate, 100 U/ml penicillin and 100 $\mu\text{g}/\text{ml}$ streptomycin. Fibroblasts were plated at 73 cells/mm². One day after plating, we treated

fibroblasts with 50 μ M tBHQ or vehicle for 18 h. Cells were trypsinized, pelleted and stored at -80°C.

Animals

GCLM-KO mice generated by Yang *et al.* (49) were bred, weaned, genotyped and maintained as described previously (32). All animal procedures were approved by the Swiss cantonal veterinary office.

Oligodendroglial cell culture and lentivirus infection

Mixed glial primary cell cultures were prepared from 1 to 3 days-old Wistar rat. Cerebral cortices were dissected and dissociated in papain solution (20 U/ml papain, 100 U/ml DNase, 1 mM L-cysteine, in L15 medium) for 30 min at 37°C, followed by mechanic dissociation. Cells derived from one brain were grown into two poly-L-ornithine-coated 75 cm² flasks in DMEM with 10% foetal calf serum and 100 U/ml penicillin-100 μ g/ml streptomycin. After 7 days, one flask was transduced with lentivirus containing the scrambled shRNA and the other with *GCLC* shRNA. Puromycin (1 μ g/ml) was added two days after cell transduction for 24 h. OPC were then isolated by a method adapted from McCarthy and Vellis (1980) (50). Briefly, flasks were shaken for 1 h at 37°C, rinsed twice with DMEM and shaken for 18 h at 37°C. Supernatant was plated in plastic dish for 45 min, afterwards OPC (supernatant) were plated in poly-L-ornithine-coated coverslips and maintained in DMEM medium supplemented with 100 U/ml penicillin-100 μ g/ml streptomycin, 2.5 μ M forskolin, 50 μ g/ml apo-transferrin, 5 μ g/ml insulin, 30 nM sodium selenate, 10 nM hydrocortisone, 10 nM D-biotin, 1 mg/ml BSA, 10 ng/ml PDGF-AA and 10 ng/ml bFGF. In late differentiation experiments, OPC were grown in medium lacking growth factors (PDGF-AA and bFGF) and supplemented with 40 ng/ml 3,3',5-triiodo-L-thyronine (thyroid hormone: T3) from 7-days after transduction. OPC

were exposed to 1 mM of N-acetylcysteine (NAC; Sigma), or 1 μ M PP1 (Fyn inhibitor; Sigma), or to vehicle for 24 h.

Antibodies

Antibodies used for immunofluorescent staining are: rabbit polyclonal anti-NG2 (1:600; Millipore), mouse monoclonal anti-O4 (1:200; Millipore), mouse monoclonal anti-CNP (1:500; Chemicon, clone 11-5B), rat monoclonal anti-MBP (1:400; Millipore), mouse monoclonal anti-APC (CC1; 1:70; Calbiochem), mouse anti-BrdU (Roche Applied Science), Cy3 goat anti-mouse IgG (1:300; Molecular Probe), Alexa488 goat anti-rabbit IgG or anti-mouse IgG (1:300; Molecular Probe), Cy3 goat anti-rat IgG (1:600; Millipore), anti-mouse-Ig-fluorescein (Roche Applied Science). For Western blot experiments, we used mouse antibody to GCLC at 1:10000 (kindly provided by P. Vliet, University of Washington, Seattle, WA), rabbit polyclonal anti-PDGFR (1:2000; Santa Cruz), mouse monoclonal anti-Fyn (1:1000; Abcam), mouse monoclonal anti-CNP (1:2000; Chemicon, clone 11-5B), mouse monoclonal anti- α -Tubulin (1:200; Santa Cruz), mouse monoclonal anti- β -actin (1:10000; Abcam), horseradish peroxidase-conjugated anti-mouse or anti-rabbit (1:10000, GE Healthcare). Mouse monoclonal antibody to Fyn (Abcam) was used for immunoprecipitate Fyn kinase protein.

Immunohistochemistry, confocal microscopy and image analysis

Forty- and 90-days-old *GCLM*-KO mice or wild-type mice were anesthetized, perfused and their brains were removed as described in Cabungcal *et al.* (51). Briefly, three consecutive sections (40 μ m) from each animal (bregma 1.14-1.34 mm) were selected, permeabilized with 0.3% Triton X-100 in 0.1 M phosphate buffer saline (PBS), and blocked for 1 h in 0.1 M PBS, 0.3% Triton X-100, 2% normal goat serum (NGS). Sections were incubated for 48 h at

4°C with the primary antibodies diluted in blocking buffer. After incubation with secondary antibodies in 0.1 M PBS, 0.3% Triton X-100 for 1 h at room temperature (RT), sections were counterstained with DAPI (4'-6-diamidino-2-phenylindole: 1.5 µM in 0.1 M PBS; Molecular Probe) for 10 min, and were mounted in Mowiol solution. Images were captured with Zeiss LSM 710 Quasar confocal microscope equipped with 40x objectives. Z-stack of 10 images was scanned. As fiber labeling with MBP and CNP was dense, the first five and last five images of the z-stack were treated separately. Images were reconstituted with Imaris 6.2 software. In ImageJ, four areas of 0.02 mm² were placed from layer I (Figure 2b). For MBP and CNP quantification, a fixed intensity threshold was applied in each area and ratio of stained pixels over the total pixel number was calculated. Each value for one area corresponds to mean of sum of both z-stack groups. For CC1 labeling, a fixed intensity threshold was applied in each area and the number of CC1 positive cells over 60 pixels was quantified. Values reported correspond to sum of CC1 positive cells in all areas.

shRNA construction and lentivirus particle production

GCLM shRNA (5'-CTCAGTCCTTGGAGTTGCA ttcaagaga TGCAACTCCAAGGACTGAG-3'), GCLC shRNA (5'-GGAGGCTACTTCTATATTA ttcaagaga TAATATAGAAGTAGCCTCC-3') and scramble shRNA (5'-CTTACAATCAGACTGGCGA ttcaagaga TCGCCAGTCTGATTGTAAG-3') were inserted in a pSP-93P vector containing puromycin resistance gene.

Human embryonic kidney 293T cells were plated and transfected the day after using calcium phosphate method with the vectors coding for virion packaging elements (5 µg pMD2.G; 15 µg pCMV-dR8.74) and vector genome (20 µg shRNA-pSP-93P). Medium was replaced 8 h after transfection. Supernatants were collected 24 h later, filtered through 0.45 µm membrane,

pelleted at 19,000 rpm for 90 min at 4°C and resuspended in DMEM. Lentivirus titration was measured with HIV-1 p24 antigen ELISA Kit (ZeptoMetrix).

Monochlorobimane assay

Cells were incubated with 100 µM monochlorobimane (Calbiochem) in HEPES buffer (140 mM NaCl, 5 mM KCl, 20 mM glucose, 2 mM CaCl₂, 10 mM HEPES, 1 mM MgCl₂, pH 7.4) and fluorescence emission (460 nm) was measured every minute for 40 min under inverted Nikon eclipse TE300 microscope, equipped with 20x objective. For quantification in MetaMorph, we selected image captured at 40 min and we subtracted background. Each value reported corresponds to mean fluorescence intensity of cells.

Survival assay

Sytox® Orange Nucleic Acid Stain (Invitrogen) was added to cells at 1 µM for 30 min at 37°C before fixation. Nuclei were labeled with DAPI for 10 min and coverslips were mounted in Mowiol solution. Four images per coverslip were captured with Axioskop2 fluorescence microscope (Zeiss) equipped with 16x objective. We calculated ratio between Sytox positive cell number and total cell number with ImageJ. Values reported correspond to mean of ratio from the four images.

Proliferation assay

OPC were treated with 10 µM BrdU (Roche Applied Science) for 4 h at 37°C. Cells were fixed, blocked (2% NGS in PBS for 30min) and immunolabeled following manufacturer instructions. After DAPI staining, coverslips were mounted in Mowiol. Images were captured using Axioskop2 fluorescence microscope (Zeiss) with a 16x objective. We analyzed four

images per condition with ImageJ. Values reported represent mean of ratio between BrdU and NG2 positive cells.

Immunocytochemistry and quantification

After fixation, cells were permeabilized with 0.1% Triton X-100 in PBS for 5 min at RT, and blocked in 0.1 M PBS, 2% NGS, 0.1% Triton X-100 for 30 min at RT. Primary antibodies were incubated in PBS, 2% NGS, 0.1% Triton X-100 for 30min at 37°C. After incubation with secondary antibodies in PBS for 30 min at 37°C, cells were counterstained with DAPI for 10 min. Coverslips were mounted in Mowiol. Four images per coverslip were captured with Axioskop2 fluorescence microscope (Zeiss) equipped with 40x objective. On each image, we quantified the ratio between immunopositive cells and total cell number using ImageJ.

Western blot

Anterior cingulate cortex from mice was incubated for 10 min on ice in extraction buffer (50 mM Tris-HCl pH7.5, 250 mM NaCl, 1% SDS, 1mM dithiothreitol, 1 mM EDTA, 0.01% phenylmethanesulfonyl fluoride and protease inhibitor cocktail (Roche)), sonicated and centrifuged 15 min at 10,000g. OPC pellets were incubated for 10 min in RIPA buffer on ice and centrifuged 15 min at 10,000g. Fibroblasts pellets were suspended in ice-cold lysis buffer (50 mM Tris-HCl pH7.5, 150 mM NaCl, 1 mM EDTA, 1% triton, 0.1% SDS, 30 mM sodium fluoride, 1 mM phenylmethanesulfonyl fluoride, 30 mM β -glycerophosphate, 0.2 mM sodium orthovanadate and protease inhibitor cocktail (Roche)) and centrifuged 15 min at 10,000g. Proteins were separated by SDS-PAGE on 10% acrylamide gels, and transferred on PVDF membrane (Hybond-P). After blocking in Tris-buffered saline (TBS), 0.1% Tween 20 (TBST), 5% milk for 1 h at RT, membranes were incubated overnight at 4°C with primary

antibodies diluted in TBST, 3% BSA. Membranes were incubated with horseradish peroxidase-conjugated secondary antibody in TBST, 0.5% milk for 1 h at RT. Peroxidase activities were detected using Amersham ECL Kit (GE Healthcare). Positive signal was analyzed and normalized to α -Tubulin or β -Actin with ImageJ.

Immunoprecipitation and Fyn kinase activity

Cell lysates (150 μ g) were pre-cleared by incubation with Dynabeads® Protein G (Invitrogen) 30 min at 4°C, prior to hybridization with 6 μ g of Fyn antibody for 1 h at RT. Complexes were pulled down with 50 μ l Dynabeads® Protein G for 30 min at RT. After immunoprecipitation, Fyn activity was measured according to manufacturer protocol (Universal Tyrosine Kinase Assay Kit: Takara).

RNA isolation and qRT-PCR

RNA were extracted using PerfectPure™ RNA cultured cell Kit (5Prime), as described in the manufacturer protocol. cDNA were synthesized using the following reaction mix: 300 ng RNA, 5.5 mM MgCl₂, 2 mM dNTP, 0.4 U/ μ l RNasin Inhibitor, 2.5 μ M Random Hexamer, 1.25 U/ μ l RTase and bufferRT 10x from Applied Biosystem. Taqman real time PCR was performed in final volume of 20 μ l containing 10 ng cDNA, 1 μ l of selected probes mixed with 10 μ l of TaqMan Universal PCR Master Mix (Applied Biosystems). Probes used were: 18S (4333760T), Fyn (Hs00941600_m1) and Fyn (Ms00941600_m1). qPCR was performed on Applied Biosystems 7500 Fast Real-Time PCR System and the 7500 Fast System SDS Software as established by the provider. Samples were run in duplicate. In animal model, data were normalized to the internal control β -Tubulin and cerebellum. Human data were normalized to the internal control 18S and analyzed using $\Delta\Delta$ Ct method (52).

Statistical analysis

Statistics were performed with R version 2.13. Data from MBP and CNP immunohistochemistry were analyzed by linear mixed-effect model. *In vitro* and *in vivo* data that followed a normal distribution (verified by Shapiro test) were analyzed by paired Student *t* test. Otherwise, a non-parametric test (Wilcoxon test) was applied. For multiple comparisons (control vs NAC or DMSO vs PP1), we used a linear mixed-effect model. Antipsychotic drug effect on GSH and Fyn was analyzed with ANOVA. Pearson correlation was used to study the relationship between GSH and both gFA and functional connectivity in control subjects. In early psychosis patients, we noticed highly non-linear relations between psychosis duration, medication dose and both gFA and functional connectivity. Consequently, Generalized Additive Model was used to measure the association between GSH and both gFA and functional connectivity, allowing a smooth semi-parametric relation between explanatory variables and the response without imposing any parametric relation on the model.

Results

Relationship between frontal GSH levels and connectivity in the human cingulum bundle

In control subjects and early psychosis patients, we investigated the relationship between medial prefrontal GSH levels measured by ¹H-MRS, and white matter integrity in the cingulum bundle assessed with Diffusion Spectrum Imaging (DSI) and the derived generalized Fractional Anisotropy (gFA) values (Figure 1a) (39). In addition, the functional connectivity along the cingulum (between the medial prefrontal cortex on one side and the isthmus of the cingulate cortex and precuneus on the other) was assessed with resting state functional MRI (Figure 1a) (53). To focus on the prefrontal maturation period, we included only individuals younger than 30-years-old (54); controls and patients were matched for age and gender (Table 1a). In control subjects, significant positive correlations between GSH levels and both gFA values and the functional connectivity along the cingulum were found ($r = 0.33$, $p = 0.03$ / $r = 0.40$, $p = 0.01$) (Figure 1b). In early psychosis patients, GSH levels were also positively associated with gFA values when medication and psychosis duration were included as covariates ($r = 0.31$, $p = 0.01$), while functional connectivity did not show any correlation with GSH levels even including these cofactors ($r = 0.21$, $p = 0.34$) (Figure 1c). These findings indicate a potential dependence between GSH levels and white matter integrity during prefrontal cortex development in control subjects and patients. Moreover, GSH levels are associated with the functional connectivity in control subjects, a mechanism likely disrupted in schizophrenia.

Low GSH affects oligodendrocyte maturation and myelination

To explore the influence of brain GSH levels on myelination in prefrontal cortex (in particular anterior cingulate cortex (Figure 2a)), we used a mouse model which has low GSH levels

(*GCLM-KO*). The immunolabeling for two myelin-associated proteins, 2',3'-cyclic-nucleotide 3'-phosphodiesterase (CNP) and myelin basic protein (MBP) were decreased in *GCLM-KO* mice as compared to wild-type animals at peripubertal age (Figure 2b, 2d; Supplementary Figure 1a, 1c) but not in adulthood (Figure 2c-d; Supplementary Figure 1b-c). Quantification revealed a reduction of MBP immunostaining of $45 \pm 15\%$ in the superficial layer (area a; see Figure 2b), $63 \pm 5\%$ in area b, $41 \pm 7\%$ in area c and $35 \pm 9\%$ in deeper area (area d) of peripubertal *GCLM-KO* mice compared to wild-type mice (Figure 2d). Similar results were obtained with CNP immunolabeling ($39 \pm 15.3\%$, $62 \pm 6.1\%$, $43 \pm 3.9\%$, $40 \pm 9.1\%$ for areas a to d) (Supplementary Figure 1c). We also quantified the number of mature oligodendrocytes labeled with CC1 marker. At peripubertal stage, the number of CC1 positive cells was reduced by $50.1 \pm 4.8\%$ in the anterior cingulate cortex of *GCLM-KO* mice (Figure 2e-f). These observations indicate a critical role of GSH levels for oligodendrocyte maturation and myelin formation during the peripubertal period.

GSH synthesis deficit impairs proliferation and maturation of OPC

To further investigate the mechanism underlying the effect of redox dysregulation on oligodendrocyte maturation, we used OPC-enriched primary cultures ($94 \pm 0.4\%$ NG2 positive cells) to assess proliferation and differentiation of OPC having lower GSH levels (Figure 3a). Deficit in intracellular GSH was induced by transducing cells with lentiviral particles containing a shRNA targeting the catalytic or modulatory subunit of GCL, the rate limiting enzyme of GSH synthesis. At 7 days post-infection, the GCLC shRNA caused a $49 \pm 5\%$ reduction in GCLC subunit as shown by Western blot (Figure 3b) and a $28 \pm 8\%$ decrease in GSH levels compared to control cells transduced with scrambled sequence shRNA (Figure 3c). The GSH decrease induced with GCLC shRNA remained stable for at least 10 days (Figure 3c). In contrast, GCLM shRNA reduced GSH levels only by $15 \pm 11\%$ (data not

shown) and thus was not further used. Proliferation of OPC was evaluated by BrdU incorporation at 7 days post-infection (Figure 3d). The double staining with BrdU and NG2 indicated that GCLC shRNA leads to a $29 \pm 7\%$ reduction in OPC proliferation as compared to scrambled shRNA (Figure 3e). To determine if the effect was due to an increase in cell death, we assessed necrosis and apoptosis levels by using Sytox dye. The number of Sytox positive cells was low and homogenous among groups, indicating that a 28% GSH decrease did not affect OPC survival (Supplementary Figure 2). N-acetylcysteine (NAC), a redox regulator and GSH precursor, prevented the decrease of proliferation induced by GSH deficit in GCLC shRNA conditions (Figure 3e), but also increased OPC proliferation by a factor of 1.7 ± 0.4 (Figure 3e).

Early differentiation of the progenitor cells occurring without exogenous differentiation factors (thyroid hormone: T3) was also assessed by immunocytolabeling of stage-specific markers: O4 for pre-oligodendrocyte and CNP for oligodendrocytes (Supplementary Figure 3). At 7 days post-infection, the density of O4- or CNP-positive cells was similar in cells transduced with GCLC or control shRNA (Figure 3f). However, at 10 days post-infection, the proportion of O4 and CNP positive cells was, respectively, 1.7 ± 0.2 and 2.7 ± 0.3 times higher in conditions with GCLC shRNA than with the control shRNA (Figure 3g). Together, this indicates that a GSH deficit promotes the switch from proliferation to early differentiation.

To evaluate the consequence of GSH deficit on a more mature oligodendrocyte stage, we cultured OPC with exogenous differentiation factors (T3) from 7 days post-infection. The level of CNP positive cells in control and GCLC shRNA OPC cultures was respectively 2.7 ± 0.4 times higher in differentiating (T3) than in proliferating medium (PDGF, bFGF) (Figure 3h). However, the number of mature oligodendrocyte labeled with MBP was reduced by $57.2 \pm 11\%$ in GSH deficit conditions (Figure 3i-j).

These observations suggest that a compromised GSH synthesis decreases proliferation, increases early differentiation of OPC but impairs oligodendrocyte maturation in a later stage. We then explored the molecular mechanism that could link GSH deficit to the impairment in oligodendrocyte maturation processes.

GSH synthesis deficit affects Fyn kinase

It has been suggested that OPC proliferation may depend on platelet-derived growth factor receptor (PDGFR)-mediated pathway and the switch from proliferation to early differentiation is in part due to a Fyn kinase-mediated degradation of PDGFR (55, 56). Therefore, we asked whether an upregulation of Fyn was responsible for the decreased proliferation in OPC transduced with GCLC shRNA. At 7 days post-infection, the levels of PDGFR protein expression were reduced by $16 \pm 5\%$ in GCLC shRNA compared to scrambled shRNA OPC cultures (Figure 4a). While there was no difference in Fyn protein levels between control and GCLC shRNA OPC (Figure 4b), a two-fold increase in Fyn kinase activity was observed under GSH deficit conditions (Figure 4c). Inhibition of Fyn with PP1 prevented the decreased proliferation of OPC induced by GCLC shRNA (Figure 4d). These results indicate that a GSH deficit leads to a reduction of OPC proliferation through an increase of Fyn kinase activity and a decrease of PDGFR protein levels *in vitro*.

Then, we investigated whether a Fyn upregulation was also present in the anterior cingulate cortex of *GCLM*-KO mice. Fyn mRNA expression was increased by 1.2 ± 0.05 times in 20-days-old but not 40- and 90-days-old *GCLM*-KO mice as compared to age-matched wild-type mice (Figure 4e). Consistently, Fyn protein levels were also increased by 1.2 ± 0.05 times in 20-days-old *GCLM*-KO mice as compared to wild-type mice (Figure 4f). These indicate that Fyn is upregulated during the development of prefrontal cortex in animal model with low GSH levels.

Abnormal Fyn mRNA and protein expression in early psychosis patient with redox impairments

We then assessed whether abnormal Fyn kinase levels were also found in early psychosis patients with a redox dysregulation. We investigated Fyn regulation in response to oxidative stress induced by *tert*-butylhydroquinone (tBHQ) in skin-derived fibroblasts. In a previous study, we found that under oxidative stress conditions, GSH levels were significantly lower in fibroblasts with “GAG high-risk” compared to “GAG low-risk” GCLC genotypes (27). This and another study on plasma thiol levels indicate that the “GAG high-risk” is associated with impaired redox regulation (29). Here, we compared Fyn mRNA expression in fibroblasts from control subjects (“GAG low-risk”), with that of early psychosis patients (“GAG low-risk” and “GAG high-risk” genotypes) (Table 1b). In absence of tBHQ, Fyn mRNA levels were homogenous in all three groups (Figure 4g). The oxidative challenge led to Fyn mRNA downregulation in fibroblasts from control subjects and “GAG low-risk” patients, as compared to vehicle treatments (Figure 4h). In contrast, no such downregulation was observed in fibroblasts of “GAG high-risk” genotypes associated with low GSH levels (Figure 4h). Likewise, Fyn protein levels were downregulated in fibroblasts from control subjects and “GAG low-risk” patients in response to tBHQ treatment (Figure 4i). However, in fibroblasts of “GAG high-risk” genotypes, Fyn protein expression was not different in response to oxidative stress (Figure 4i). In conclusion, fibroblasts from schizophrenia patients with a genetic risk for an abnormal redox regulation also display an impaired regulation of Fyn mRNA and protein expressions.

Discussion

The present study highlights an important role of GSH for oligodendrocyte differentiation and myelination processes. We found that GSH levels measured in the medial prefrontal cortex are positively associated with white matter integrity in the cingulum bundle of young healthy subjects and early psychosis patients. In the anterior cingulate cortex of peripubertal *GCLM*-KO mice, a constitutive GSH deficit causes reduced expression of myelin-associated proteins and decreased number of mature oligodendrocytes. Using OPC cultures, we found that a deficit in GSH decreases OPC proliferation via Fyn upregulation, and it also impairs oligodendrocyte maturation. Consistently, fibroblasts of patients carrying “GAG high-risk” genotypes in the *GCLC* gene, which are associated with a phenotype of redox dysregulation, present abnormal regulation of Fyn when challenged with an oxidative stress.

Our observation that a GSH deficit decreases OPC proliferation and promotes early differentiation is in agreement with previous studies showing a switch from OPC division to early differentiation following treatment with either buthionine sulfoximine (BSO), an inhibitor of GSH synthesis, or pro-oxidants (i.e. methylmercury, lead, paraquat) in absence of differentiating factors in the medium (55, 56). However, when differentiating factors are added to the medium, a deficit in GSH induced either by *GCLC* shRNA (this study) or BSO (57) impairs oligodendrocyte maturation. These latter *in vitro* data are consistent with the impaired oligodendrocyte and myelination observed in *GCLM*-KO mice. Moreover, these data are further supported by the positive relationship between GSH levels and gFA along the cingulum bundle in young healthy subjects and early psychosis patients. This suggest a role for GSH during the development of fibers, either at the level of myelin or axonal size or fiber packing since gFA can be influenced by these various factors (58). Together, these suggest that a proper timing of redox regulation and differentiation signals is crucial to control the proliferation and the various stages of oligodendrocyte differentiation. Thus, an imbalance

between ROS and antioxidant systems could therefore affect myelination processes and white matter integrity along various developmental periods.

Myelination of the prefrontal lobe progresses through adolescence and completes only in early adulthood (59-61). Although the dynamics of this process may be different in rodents, our observation that *GCLM*-KO mice present a myelin deficit in the anterior cingulate cortex during peripubertal period and no myelin impairment at adulthood suggests that this latter is a vulnerable time period during which an adequate redox control is required. In agreement with this interpretation, a transcriptomic study in the prefrontal cortex identified genes for which expression profiles specifically peak during late adolescence through early adulthood (i.e. between ages 15 and 25 years). Besides genes related to either myelin or lipid synthesis, the antioxidant response system is one of the most highly expressed during this period (60). In line with this, we found a positive association between GSH levels and gFA only when individuals under 30 years of age were included. This corresponds to an age until which the cingulum bundle is still maturing (54). Early adulthood coincides with the mean onset of schizophrenia and the development of higher cognitive processes such as executive function and social cognitive function (62), both of which are affected in the disease. We propose that a redox dysregulation during the period of myelin maturation could lead to disrupted connectivity in the prefrontal cortex and contribute later in the appearance of the symptoms. Moreover, oligodendrocyte and myelin impairments may be implicated in cognitive dysfunction (63, 64).

In control subjects, GSH levels also positively correlate with the functional connectivity between the medial prefrontal and the posterior cingulate cortices in control. Therefore, higher GSH levels correspond to better synchronization of these two areas, in line with their higher gFA values.

Finally, our study reveals that a GSH deficit causes an impairment of Fyn pathway. A GSH deficit results in decreased proliferation in OPC culture via the upregulation of Fyn kinase activity. Likewise, young *GCLM*-KO mice have an increase in Fyn mRNA and protein expressions in the developing anterior cingulate cortex. The upregulation of Fyn in our *in vitro* and *in vivo* models of GSH deficit is also in line with redox regulation of Fyn activity described in various cell types, including lymphocytes, endothelial cells and fibroblasts (65, 66). Interestingly, fibroblasts from early psychosis patients with “GAG high-risk” genotypes, associated with a vulnerability to redox dysregulation, have impaired regulation of Fyn mRNA and protein expressions during an oxidative challenge (tBHQ). Noteworthy, an increase in Fyn mRNA and protein levels has been also reported in *postmortem* prefrontal cortex of schizophrenia patients (67). Furthermore, the Stanley Neuropathology Consortium Integrative Database (a web-based tool that integrates results of various microarray studies done with the Stanley brain array collection: <https://www.stanleygenomics.org/>) reveals a significant upregulation of Fyn mRNA expression in schizophrenia patients (35 cases *vs.* 35 controls). To summarize, the increase of Fyn in a patients’ subgroup may result from an impairment in redox regulation, and cause impaired Fyn-mediated signaling pathways that could contribute to developmental abnormalities including oligodendrocyte maturation.

All together, these data suggest the presence of a critical developmental period during which a proper redox regulation and GSH levels are required for myelination processes. Adverse events during early life are risk factors for the psychopathology and myelin development (68, 69). This also suggests that there are several critical periods during which environmental risk factors could impact the normal development of myelin. Indeed, transient changes in GSH levels induced by environmental insults during pre-, peri- and post-natal periods may have an impact on oligodendrocyte maturation, consequently affecting later structural connectivity.

A better understanding of molecular mechanisms underlying redox control of myelination at various developmental vulnerability periods will pave the way towards new drug targets and strategies for the treatment and prevention of schizophrenia.

Acknowledgments

This work was supported by the Swiss National Science Foundation (grants n° 310030_135736/1 to KQ.D. and P.S., 320030_122419 to P.C. and KQ.D., 130090 to P.H., and 320030-130090 to A.G.) and National Center of Competence in Research (NCCR) “SYNAPSY - The Synaptic Bases of Mental Diseases” (grants n° 51AU40_125759). We also thank the Brazilian Swiss Joint Research Program (BSJRP), the “Loterie Romande”, Damm-Etienne Foundation, Avina Foundation and Alamaya Foundation. P.H. was financially supported by Leenaards Foundation. We are grateful for technical assistance to Hélène Moser and Adeline Cottier. We thank Dr Mehdi Gholam for advices on statistics, Dr Portia Vliet for the GCLC antibody and Dr Ibro Ambeskovic for advices on OPC culture and *in vitro* experiments. We also thank Ying Chen for providing us with the *GCLM*-KO breeders. Most of all, we express our gratitude to all patients and healthy volunteers for their enduring participation.

Author contributions

A.M. wrote the manuscript, designed and carried out the rodent experiments, and performed human fibroblast culture. PS.B. wrote the manuscript and performed the patient recruitment and skin biopsy, and analyzed DSI. A.G. performed DSI/fMRI acquisition and analyzed the data. L.X. and R.M. performed MRS acquisition and analyzed the data. M.F. wrote the manuscript, designed and performed human fibroblast culture, and evaluated data from Stanley database. C.B. designed and prepared shRNA. M.K. established OPC culture. J-H.C. contributed to morphology analysis of *GCLM*-KO mice and editing the manuscript. P.S. designed and contributed to experiments in rodents and to the manuscript writing. C.F. recruited control subjects and early psychosis patients and performed psychiatric evaluations. M.C. contributed to the overall study concept and to the manuscript writing. R.G. supervised

MRS study. J-P.T. supervised DSI/fMRI analysis. P.H. designed, analyzed and supervised DSI/fMRI study. P.C. contributed to the overall concept, planned and coordinated the recruitment in human study. KQ.D. conceived and directed the whole study, and contributed to the writing. All authors reviewed and edited the manuscript.

Competing financial interests

The authors declare no competing financial interests.

Table 1 Demographic information for control subjects and early psychosis patients.**a. MRI study**

	Control subjects	Patients	p value
	(n=40)	(n=30)	
Age (years ± s.d.)	23.5 ± 3.2	23.1 ± 3.5	0.7 ^a
Gender	25 men; 15 women	19 men; 11 women	1.0 ^b
CPZ equivalent (mg ± s.d.)	NA	330.3 ^c ± 218.9	NA
Psychosis duration (years ± s.d.)	NA	2.0 ± 1.8	NA

^aIndependent two tailed Student *t* test; ^bchi-square; ^ctwo patients without antipsychotic medication; NA: not applicable; CPZ: chlorpromazine equivalents

b. Fyn mRNA study

	Control subjects	“GAG low-risk” patients	“GAG high-risk” patients	p value^a
	(n=15)	(n=14)	(n=14)	
Age (years ± s.d.)	25.7 ± 6.3	23.0 ± 3.3	23.4 ± 3.4	0.23
Gender	15 men	14 men	14 men	NA
CPZ equivalent (mg ± s.d.)	N/A	358.4 ^b ± 197.1	271.8 ^c ± 149.9	NA

^aOne way anova; ^bone patient without antipsychotic medication; ^cthree patients without antipsychotic medication; CPZ: chlorpromazine equivalents; NA: not applicable

c. Fyn protein study

	Control subjects	“GAG low-risk” patients	“GAG high-risk” patients	p value^a
	(n=12)	(n=10)	(n=10)	
Age (years ± s.d.)	24.2 ± 3.1	23.0 ± 3.7	22.9 ± 2.8	0.57
Gender	12 men	10 men	10 men	NA
CPZ equivalent (mg ± s.d.)	N/A	361.0 ± 218.2	284.6 ^b ± 200.7	NA

^aOne way anova; ^btwo patients without antipsychotic medication; CPZ: chlorpromazine equivalents; NA: not applicable

References

1. Davis KL, Stewart DG, Friedman JI, Buchsbaum M, Harvey PD, Hof PR *et al.* White matter changes in schizophrenia: evidence for myelin-related dysfunction. *Archives of general psychiatry* 2003 May;**60**(5):443-456.
2. Hakak Y, Walker JR, Li C, Wong WH, Davis KL, Buxbaum JD *et al.* Genome-wide expression analysis reveals dysregulation of myelination-related genes in chronic schizophrenia. *Proceedings of the National Academy of Sciences of the United States of America* 2001 Apr 10;**98**(8):4746-4751.
3. Katsel P, Davis KL, Haroutunian V. Variations in myelin and oligodendrocyte-related gene expression across multiple brain regions in schizophrenia: a gene ontology study. *Schizophrenia research* 2005 Nov 15;**79**(2-3):157-173.
4. Hof PR, Haroutunian V, Copland C, Davis KL, Buxbaum JD. Molecular and cellular evidence for an oligodendrocyte abnormality in schizophrenia. *Neurochemical research* 2002 Oct;**27**(10):1193-1200.
5. Stark AK, Uylings HB, Sanz-Arigitia E, Pakkenberg B. Glial cell loss in the anterior cingulate cortex, a subregion of the prefrontal cortex, in subjects with schizophrenia. *The American journal of psychiatry* 2004 May;**161**(5):882-888.
6. Uranova NA, Vostrikov VM, Vikhreva OV, Zimina IS, Kolomeets NS, Orlovskaya DD. The role of oligodendrocyte pathology in schizophrenia. *The international journal of neuropsychopharmacology / official scientific journal of the Collegium Internationale Neuropsychopharmacologicum* 2007 Aug;**10**(4):537-545.
7. Du F, Cooper A, Cohen BM, Renshaw PF, Ongur D. Water and metabolite transverse T2 relaxation time abnormalities in the white matter in schizophrenia. *Schizophrenia research* 2012 May;**137**(1-3):241-245.
8. Kubicki M, Westin CF, McCarley RW, Shenton ME. The application of DTI to investigate white matter abnormalities in schizophrenia. *Annals of the New York Academy of Sciences* 2005 Dec;**1064**:134-148.
9. Kyriakopoulos M, Bargiotas T, Barker GJ, Frangou S. Diffusion tensor imaging in schizophrenia. *Eur Psychiatry* 2008 Jun;**23**(4):255-273.
10. Bitanihirwe BK, Woo TU. Oxidative stress in schizophrenia: an integrated approach. *Neuroscience and biobehavioral reviews* 2011 Jan;**35**(3):878-893.
11. Do KQ, Cabungcal JH, Frank A, Steullet P, Cuenod M. Redox dysregulation, neurodevelopment, and schizophrenia. *Current opinion in neurobiology* 2009 Apr;**19**(2):220-230.
12. Reddy R, Keshavan M, Yao JK. Reduced plasma antioxidants in first-episode patients with schizophrenia. *Schizophrenia research* 2003 Aug 1;**62**(3):205-212.
13. Yao JK, Keshavan MS. Antioxidants, redox signaling, and pathophysiology in schizophrenia: an integrative view. *Antioxidants & redox signaling* 2011 Oct 1;**15**(7):2011-2035.
14. Jones DP. Radical-free biology of oxidative stress. *American journal of physiology Cell physiology* 2008 Oct;**295**(4):C849-868.
15. Meister A, Anderson ME. Glutathione. *Annu Rev Biochem* 1983;**52**:711-760.
16. Do KQ, Trabesinger AH, Kirsten-Kruger M, Lauer CJ, Dydak U, Hell D *et al.* Schizophrenia: glutathione deficit in cerebrospinal fluid and prefrontal cortex in vivo. *The European journal of neuroscience* 2000 Oct;**12**(10):3721-3728.
17. Matsuzawa D, Hashimoto K. Magnetic resonance spectroscopy study of the antioxidant defense system in schizophrenia. *Antioxidants & redox signaling* 2011 Oct 1;**15**(7):2057-2065.

18. Gawryluk JW, Wang JF, Andrezza AC, Shao L, Young LT. Decreased levels of glutathione, the major brain antioxidant, in post-mortem prefrontal cortex from patients with psychiatric disorders. *The international journal of neuropsychopharmacology / official scientific journal of the Collegium Internationale Neuropsychopharmacologicum* 2011 Feb;**14**(1):123-130.
19. Krishnan N, Dickman MB, Becker DF. Proline modulates the intracellular redox environment and protects mammalian cells against oxidative stress. *Free radical biology & medicine* 2008 Feb 15;**44**(4):671-681.
20. Millar JK, Christie S, Semple CA, Porteous DJ. Chromosomal location and genomic structure of the human translin-associated factor X gene (TRAX; TSNAX) revealed by intergenic splicing to DISC1, a gene disrupted by a translocation segregating with schizophrenia. *Genomics* 2000 Jul 1;**67**(1):69-77.
21. Otte DM, Sommersberg B, Kudin A, Guerrero C, Albayram O, Filiou MD *et al.* N-acetyl cysteine treatment rescues cognitive deficits induced by mitochondrial dysfunction in G72/G30 transgenic mice. *Neuropsychopharmacology : official publication of the American College of Neuropsychopharmacology* 2011 Oct;**36**(11):2233-2243.
22. Straub RE, Jiang Y, MacLean CJ, Ma Y, Webb BT, Myakishev MV *et al.* Genetic variation in the 6p22.3 gene DTNBP1, the human ortholog of the mouse dysbindin gene, is associated with schizophrenia. *American journal of human genetics* 2002 Aug;**71**(2):337-348.
23. Stefansson H, Sigurdsson E, Steinthorsdottir V, Bjornsdottir S, Sigmundsson T, Ghosh S *et al.* Neuregulin 1 and susceptibility to schizophrenia. *American journal of human genetics* 2002 Oct;**71**(4):877-892.
24. Gokhale A, Larimore J, Werner E, So L, Moreno-De-Luca A, Lese-Martin C *et al.* Quantitative proteomic and genetic analyses of the schizophrenia susceptibility factor dysbindin identify novel roles of the biogenesis of lysosome-related organelles complex 1. *The Journal of neuroscience : the official journal of the Society for Neuroscience* 2012 Mar 14;**32**(11):3697-3711.
25. Goldshmit Y, Erlich S, Pinkas-Kramarski R. Neuregulin rescues PC12-ErbB4 cells from cell death induced by H₂O₂. Regulation of reactive oxygen species levels by phosphatidylinositol 3-kinase. *The Journal of biological chemistry* 2001 Dec 7;**276**(49):46379-46385.
26. Park YU, Jeong J, Lee H, Mun JY, Kim JH, Lee JS *et al.* Disrupted-in-schizophrenia 1 (DISC1) plays essential roles in mitochondria in collaboration with Mitofilin. *Proceedings of the National Academy of Sciences of the United States of America* 2010 Oct 12;**107**(41):17785-17790.
27. Gysin R, Kraftsik R, Sandell J, Bovet P, Chappuis C, Conus P *et al.* Impaired glutathione synthesis in schizophrenia: convergent genetic and functional evidence. *Proceedings of the National Academy of Sciences of the United States of America* 2007 Oct 16;**104**(42):16621-16626.
28. Tomic M, Ott J, Barral S, Bovet P, Deppen P, Gheorghita F *et al.* Schizophrenia and oxidative stress: glutamate cysteine ligase modifier as a susceptibility gene. *American journal of human genetics* 2006 Sep;**79**(3):586-592.
29. Gysin R, Kraftsik R, Boulat O, Bovet P, Conus P, Comte-Krieger E *et al.* Genetic dysregulation of glutathione synthesis predicts alteration of plasma thiol redox status in schizophrenia. *Antioxidants & redox signaling* 2011 Oct 1;**15**(7):2003-2010.
30. Steullet P, Cabungcal JH, Kulak A, Kraftsik R, Chen Y, Dalton TP *et al.* Redox dysregulation affects the ventral but not dorsal hippocampus: impairment of parvalbumin neurons, gamma oscillations, and related behaviors. *The Journal of neuroscience : the official journal of the Society for Neuroscience* 2010 Feb 17;**30**(7):2547-2558.

31. Cabungcal JH, Steullet P, Kraftsik R, Cuenod M, Do KQ. Early-Life Insults Impair Parvalbumin Interneurons via Oxidative Stress: Reversal by N-Acetylcysteine. *Biological psychiatry* 2012 Nov 6.
32. Kulak A, Cuenod M, Do KQ. Behavioral phenotyping of glutathione-deficient mice: relevance to schizophrenia and bipolar disorder. *Behavioural brain research* 2012 Jan 15;**226**(2):563-570.
33. Thorburne SK, Juurlink BH. Low glutathione and high iron govern the susceptibility of oligodendroglial precursors to oxidative stress. *Journal of neurochemistry* 1996 Sep;**67**(3):1014-1022.
34. Boullerne AI, Nedelkoska L, Benjamins JA. Synergism of nitric oxide and iron in killing the transformed murine oligodendrocyte cell line N20.1. *Journal of neurochemistry* 1999 Mar;**72**(3):1050-1060.
35. Back SA, Gan X, Li Y, Rosenberg PA, Volpe JJ. Maturation-dependent vulnerability of oligodendrocytes to oxidative stress-induced death caused by glutathione depletion. *The Journal of neuroscience : the official journal of the Society for Neuroscience* 1998 Aug 15;**18**(16):6241-6253.
36. Yung AR, Yuen HP, McGorry PD, Phillips LJ, Kelly D, Dell'Olio M *et al.* Mapping the onset of psychosis: the Comprehensive Assessment of At-Risk Mental States. *Aust N Z J Psychiatry* 2005 Nov-Dec;**39**(11-12):964-971.
37. Baumann PS, Crespi S, Marion-Veyron R, Solida A, Thonney J, Favrod J *et al.* Treatment and early intervention in psychosis program (TIPP-Lausanne): implementation of an early intervention programme for psychosis in Switzerland. *Early Interv Psychiatry* 2013 Aug;**7**(3):322-328.
38. Nurnberger JI, Jr., Blehar MC, Kaufmann CA, York-Cooler C, Simpson SG, Harkavy-Friedman J *et al.* Diagnostic interview for genetic studies. Rationale, unique features, and training. NIMH Genetics Initiative. *Archives of general psychiatry* 1994 Nov;**51**(11):849-859; discussion 863-844.
39. Wedeen VJ, Hagmann P, Tseng WY, Reese TG, Weisskoff RM. Mapping complex tissue architecture with diffusion spectrum magnetic resonance imaging. *Magnetic resonance in medicine : official journal of the Society of Magnetic Resonance in Medicine / Society of Magnetic Resonance in Medicine* 2005 Dec;**54**(6):1377-1386.
40. Daducci A, Gerhard S, Griffa A, Lemkaddem A, Cammoun L, Gigandet X *et al.* The connectome mapper: an open-source processing pipeline to map connectomes with MRI. *PloS one* 2012;**7**(12):e48121.
41. Richiardi J, Eryilmaz H, Schwartz S, Vuilleumier P, Van De Ville D. Decoding brain states from fMRI connectivity graphs. *NeuroImage* 2011 May 15;**56**(2):616-626.
42. Desikan RS, Segonne F, Fischl B, Quinn BT, Dickerson BC, Blacker D *et al.* An automated labeling system for subdividing the human cerebral cortex on MRI scans into gyral based regions of interest. *NeuroImage* 2006 Jul 1;**31**(3):968-980.
43. Greicius MD, Supekar K, Menon V, Dougherty RF. Resting-state functional connectivity reflects structural connectivity in the default mode network. *Cereb Cortex* 2009 Jan;**19**(1):72-78.
44. Gruetter R. Automatic, localized in vivo adjustment of all first- and second-order shim coils. *Magnetic resonance in medicine : official journal of the Society of Magnetic Resonance in Medicine / Society of Magnetic Resonance in Medicine* 1993 Jun;**29**(6):804-811.
45. Mekle R, Mlynarik V, Gambarota G, Hergt M, Krueger G, Gruetter R. MR spectroscopy of the human brain with enhanced signal intensity at ultrashort echo times on a clinical platform at 3T and 7T. *Magnetic resonance in medicine : official journal of the Society of Magnetic Resonance in Medicine / Society of Magnetic Resonance in Medicine* 2009 Jun;**61**(6):1279-1285.

46. Mlynarik V, Gambarota G, Frenkel H, Gruetter R. Localized short-echo-time proton MR spectroscopy with full signal-intensity acquisition. *Magnetic resonance in medicine : official journal of the Society of Magnetic Resonance in Medicine / Society of Magnetic Resonance in Medicine* 2006 Nov;**56**(5):965-970.
47. Provencher SW. Estimation of metabolite concentrations from localized in vivo proton NMR spectra. *Magnetic resonance in medicine : official journal of the Society of Magnetic Resonance in Medicine / Society of Magnetic Resonance in Medicine* 1993 Dec;**30**(6):672-679.
48. Xin L, Gambarota G, Mlynarik V, Gruetter R. Proton T2 relaxation time of J-coupled cerebral metabolites in rat brain at 9.4 T. *NMR in biomedicine* 2008 May;**21**(4):396-401.
49. Yang Y, Dieter MZ, Chen Y, Shertzer HG, Nebert DW, Dalton TP. Initial characterization of the glutamate-cysteine ligase modifier subunit Gclm(-/-) knockout mouse. Novel model system for a severely compromised oxidative stress response. *The Journal of biological chemistry* 2002 Dec 20;**277**(51):49446-49452.
50. McCarthy KD, de Vellis J. Preparation of separate astroglial and oligodendroglial cell cultures from rat cerebral tissue. *The Journal of cell biology* 1980 Jun;**85**(3):890-902.
51. Cabungcal JH, Nicolas D, Kraftsik R, Cuenod M, Do KQ, Hornung JP. Glutathione deficit during development induces anomalies in the rat anterior cingulate GABAergic neurons: Relevance to schizophrenia. *Neurobiology of disease* 2006 Jun;**22**(3):624-637.
52. Livak KJ, Schmittgen TD. Analysis of relative gene expression data using real-time quantitative PCR and the 2(-Delta Delta C(T)) Method. *Methods* 2001 Dec;**25**(4):402-408.
53. Lowe MJ, Mock BJ, Sorenson JA. Functional connectivity in single and multislice echoplanar imaging using resting-state fluctuations. *NeuroImage* 1998 Feb;**7**(2):119-132.
54. Lebel C, Beaulieu C. Longitudinal development of human brain wiring continues from childhood into adulthood. *The Journal of neuroscience : the official journal of the Society for Neuroscience* 2011 Jul 27;**31**(30):10937-10947.
55. Li Z, Dong T, Proschel C, Noble M. Chemically diverse toxicants converge on Fyn and c-Cbl to disrupt precursor cell function. *PLoS biology* 2007 Feb;**5**(2):e35.
56. Noble M, Smith J, Power J, Mayer-Proschel M. Redox state as a central modulator of precursor cell function. *Annals of the New York Academy of Sciences* 2003 Jun;**991**:251-271.
57. French HM, Reid M, Mamontov P, Simmons RA, Grinspan JB. Oxidative stress disrupts oligodendrocyte maturation. *Journal of neuroscience research* 2009 Nov 1;**87**(14):3076-3087.
58. Beaulieu C. The basis of anisotropic water diffusion in the nervous system - a technical review. *NMR in biomedicine* 2002 Nov-Dec;**15**(7-8):435-455.
59. Bartzokis G. Schizophrenia: breakdown in the well-regulated lifelong process of brain development and maturation. *Neuropsychopharmacology : official publication of the American College of Neuropsychopharmacology* 2002 Oct;**27**(4):672-683.
60. Harris LW, Lockstone HE, Khaitovich P, Weickert CS, Webster MJ, Bahn S. Gene expression in the prefrontal cortex during adolescence: implications for the onset of schizophrenia. *BMC medical genomics* 2009;**2**:28.
61. Kolb B, Mychasiuk R, Muhammad A, Li Y, Frost DO, Gibb R. Experience and the developing prefrontal cortex. *Proceedings of the National Academy of Sciences of the United States of America* 2012 Oct 16;**109** Suppl 2:17186-17193.
62. Blakemore SJ, Choudhury S. Development of the adolescent brain: implications for executive function and social cognition. *Journal of child psychology and psychiatry, and allied disciplines* 2006 Mar-Apr;**47**(3-4):296-312.
63. Fields RD. White matter in learning, cognition and psychiatric disorders. *Trends in neurosciences* 2008 Jul;**31**(7):361-370.

64. Nave KA. Myelination and support of axonal integrity by glia. *Nature* 2010 Nov 11;**468**(7321):244-252.
65. Abe J, Okuda M, Huang Q, Yoshizumi M, Berk BC. Reactive oxygen species activate p90 ribosomal S6 kinase via Fyn and Ras. *The Journal of biological chemistry* 2000 Jan 21;**275**(3):1739-1748.
66. Sanguinetti AR, Cao H, Corley Mastick C. Fyn is required for oxidative- and hyperosmotic-stress-induced tyrosine phosphorylation of caveolin-1. *The Biochemical journal* 2003 Nov 15;**376**(Pt 1):159-168.
67. Ohnuma T, Kato H, Arai H, McKenna PJ, Emson PC. Expression of Fyn, a non-receptor tyrosine kinase in prefrontal cortex from patients with schizophrenia and its correlation with clinical onset. *Brain research Molecular brain research* 2003 Apr 10;**112**(1-2):90-94.
68. Eluvathingal TJ, Chugani HT, Behen ME, Juhasz C, Muzik O, Maqbool M *et al.* Abnormal brain connectivity in children after early severe socioemotional deprivation: a diffusion tensor imaging study. *Pediatrics* 2006 Jun;**117**(6):2093-2100.
69. Huang H, Gundapuneedi T, Rao U. White matter disruptions in adolescents exposed to childhood maltreatment and vulnerability to psychopathology. *Neuropsychopharmacology : official publication of the American College of Neuropsychopharmacology* 2012 Nov;**37**(12):2693-2701.

Figure legends

Figure 1 Association between GSH levels in the medial prefrontal cortex and white matter integrity (gFA) and functional connectivity along the human cingulum bundle. (a) Representation of the cingulum bundle in green, illustrating the white matter tract along which the gFA values have been averaged. Red box indicates the VOI used for GSH level measurement. The cingulate cortical regions considered for the evaluation of the functional connectivity through the cingulum are represented in orange, and include the medial prefrontal cortex, the isthmus of the cingulate cortex and the precuneus. (b-c) Scatter plots of medial prefrontal GSH levels and both gFA values (top panels) and functional connectivity (bottom panels) along the cingulum bundle in control subjects (b) and early psychosis patients (c). Each point in the scatter plots represents one subject and red lines represent confidence intervals. * $P < 0.05$ with Pearson correlation and Generalized Additive Model.

Figure 2 Forty-days-old *GCLM*-KO mice present a decreased immunoreactivity for the myelin-associated protein MBP and the mature oligodendrocyte marker CC1 in the anterior cingulate cortex. (a) Schematic drawing of coronal section with anterior cingulate cortex including in the red square, illustrating the region analyzed in panel b, c and d. (b-c) Confocal images showing MBP labeling in wild-type and *GCLM*-KO mice. White box magnified images indicate four different areas (yellow box) of 0.02 mm^2 placed from layer I, and used to quantify MBP labeling at 40-days-old (b) and 90-days-old (c). Scale bar: $50 \mu\text{m}$. (d) Quantification of MBP positive pixels in each delimited area for wild-type (diamond) and *GCLM*-KO (square) mice at 40-days-old (red) and 90-days-old (black) ($n=6-8$ animals per group). Data are expressed as mean \pm s.e.m. * $P < 0.05$, analyzed by linear mixed-effect model. (e) Confocal images showing mature oligodendrocytes labeled with CC1. Scale bar: $50 \mu\text{m}$. (f) Quantification of CC1 positive cells in area of 0.08 mm^2 including layer I to layer IV ($n=6$

animals per group). Data are expressed as mean \pm s.e.m. $**P<0.01$, analyzed by Student's *t* test.

Figure 3 GSH deficit induced by GCLC shRNA reduces proliferation, increases early differentiation but decreases later maturation stage of OPC. **(a)** Oligodendrocyte cell culture immunostained for NG2 (green) and cell nuclei counterstained with DAPI (blue). Scale bar: 50 μ m. **(b)** Quantification by Western blot of GCLC protein levels in oligodendrocyte cultures treated with either scrambled or GCLC shRNA. GCLC protein levels were normalized to α -Tubulin and expressed as percentage of their respective scrambled shRNA. Bar graphs represent mean \pm s.e.m. (n=6). $**P<0.01$. Student's paired *t* test. **(c)** GSH levels at different post-infection time 5, 7 or 10 days (n=6-7) measured by amount of fluorescence produced by GSH-monochlorobimane. Values are expressed as percentage of their respective scrambled shRNA. Bar graphs represent mean \pm s.e.m. $*P<0.05$, $**P<0.01$. Student's paired *t* test. **(d)** Proliferation of OPC assessed by BrdU incorporation (green) and co-staining with NG2 (red) and cell nuclei (DAPI: blue). Scale bar: 50 μ m. **(e)** Effect of NAC treatment (24 h) on the number of BrdU positive among NG2 positive cells. Data are expressed as percentage of their respective scrambled shRNA (n=10, mean \pm s.e.m.). $**P<0.01$, $***P<0.001$, analyzed by Wilcoxon test for control condition and linear mixed-effect model for multiple comparisons (control vs NAC). **(f-g)** Quantification of O4 and CNP positive cells over total cell nuclei (DAPI) at 7 **(f)** and 10 days **(g)** post-infection. Values were expressed as percentage of their respective control condition. Bar graphs represent mean \pm s.e.m. (n=6-7). $*P<0.05$, $**P<0.01$, analyzed by Student's paired *t* test. **(h)** Quantification of CNP protein levels in cells treated with either scrambled or GCLC shRNA in either proliferating medium (PDGF, bFGF) or differentiating medium (T3). CNP protein levels were normalized to α -Tubulin and expressed as percentage of their respective control condition (PDGF, bFGF). Bar graphs represent mean \pm s.e.m. (n=5). $**P<0.01$, analyzed by Student's paired *t* test. **(i)**

Representative image of MBP labeling (red) and cell nuclei (DAPI: blue) in oligodendrocytes expressing scrambled (top panel) or GCLC shRNA (bottom panel) following T3 incubation. Scale bar: 50 μ m. (j) Quantification of MBP positive cells over total cell nuclei after T3 treatment. Values were expressed as percentage of their respective scrambled shRNA. Bar graphs represent mean \pm s.e.m. (n=6). * P <0.05, analyzed by Student's paired t test.

Figure 4 GSH deficit affects Fyn kinase in rodents and patients. (a) PDGFR protein expression was evaluated by Western blot at 7 days post-infection (n=7). Protein levels of PDGFR were normalized to α -Tubulin and expressed as percentage of their respective scrambled shRNA (black bar). Bar graphs represent means of seven different experiments \pm s.e.m. * P <0.05, Student's paired t test. (b) Representative Western blot of Fyn protein expression at 7 days post-infection. (c) Analysis of Fyn kinase activity. Bar graphs represent Fyn-dependent ATP consumption, expressed as percentage of the scrambled condition. Bar graphs represent mean \pm s.e.m. (n=5). * P <0.05, Student's paired t test. (d) Effect of Fyn inhibitor (PP1) on proliferation assessed by BrdU incorporation. BrdU positive over NG2 positive cells were quantified after 24 h treatment with PP1 at day 7. Data are expressed as percentage of their respective scrambled shRNA treated with vehicle (DMSO) (mean \pm s.e.m., n=9). * P <0.05, linear mixed-effect model. (e) Fyn mRNA expression in anterior cingulate cortex of wild-type and *GCLM*-KO mice at 20-, 40- and 90-days-old. Data were expressed as mean \pm s.e.m., relative to wild-type mice (n=6-9). * P <0.05, Wilcoxon test. (f) Quantification by Western blot of Fyn protein levels in anterior cingulate cortex of wild-type and *GCLM*-KO mice at 20-days-old. Fyn protein levels were normalized to β -Actin. Data were expressed as mean \pm s.e.m., relative to wild-type mice (n=6-8). ** P <0.01, Student's t test. (g) Fyn mRNA expression assessed by quantitative PCR in vehicle condition (DMSO) in fibroblasts from "GAG high-risk" patients, "GAG low-risk" patients or control individuals. Mean delta Ct value is shown in bar graphs (\pm s.e.m.). (h) Fold change in Fyn mRNA expression in

fibroblasts following tBHQ treatment. Mean values of fold change relative to DMSO treatment (\pm s.e.m.). * P <0.05, ** P <0.01 Student's paired t test or Wilcoxon test. (i) Fibroblast Fyn protein expression analyzed by Western blot following tBHQ treatment. Fyn protein expression was normalized by β -Actin. Data were expressed as mean \pm s.e.m. (n=10-12), relative to vehicle condition (DMSO). * P <0.05, *** P <0.001, Student's paired t test or Wilcoxon test.

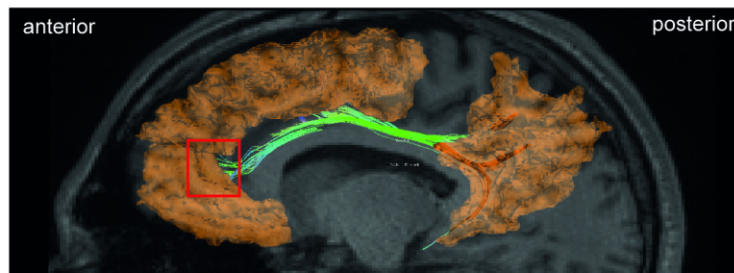
Supplementary Figure 1 Decreased immunoreactivity for the myelin-associated protein CNP in the anterior cingulate cortex of 40-days-old *GCLM*-KO mice. (a-b) Confocal images showing CNP immunolabeling at 40-days-old (a) and 90-days-old (b). Region analyzed in panel c was delimited by white box. Scale bar: 50 μ m. (c) Quantification of CNP positive pixels at 40-days-old (red) and 90-days-old (black) in four areas (a, b, c, d) defined in delimited white box. (n=6-8 animals per group). Data are expressed as mean \pm s.e.m. * P <0.05, analyzed by linear mixed-effect model.

Supplementary Figure 2 GCLC shRNA does not affect apoptosis/necrosis levels in OPC. (a) Cell death assessed by Sytox incorporation followed by counterstaining of cell nuclei (DAPI: blue). Scale bar: 50 μ m. (b) Percentage of Sytox positive cell nuclei. Data are expressed as mean \pm s.e.m. (n=7). Student's paired t test.

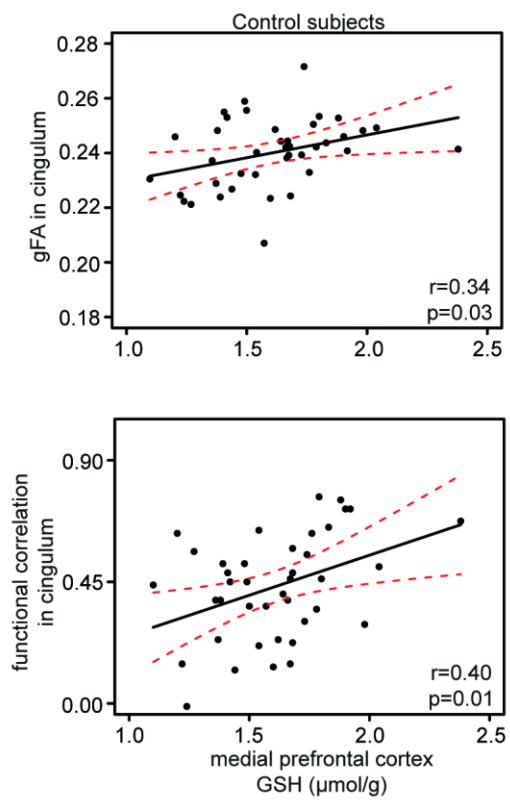
Supplementary Figure 3 GCLC shRNA enhances early differentiation of OPC. Representative images of O4 (red), CNP (red) labeling and cell nuclei (DAPI: blue) in oligodendrocytes expressing scrambled (top panel) or GCLC shRNA (bottom panel) at day 10. Scale bar: 50 μ m.

Figure 1

a



b



c

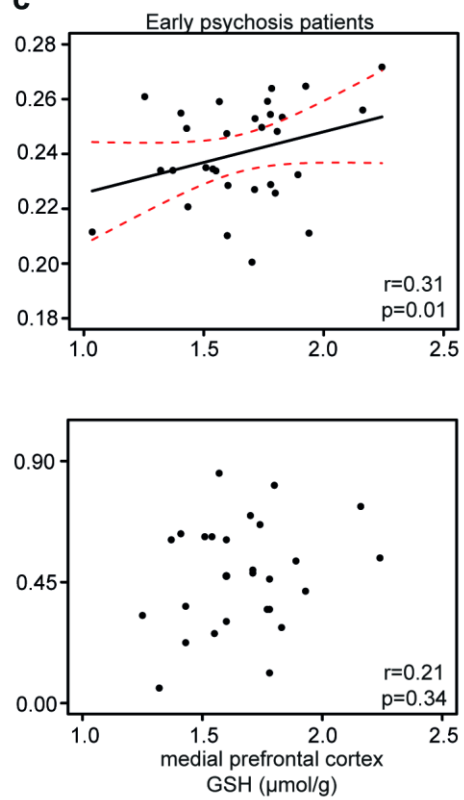


Figure 2

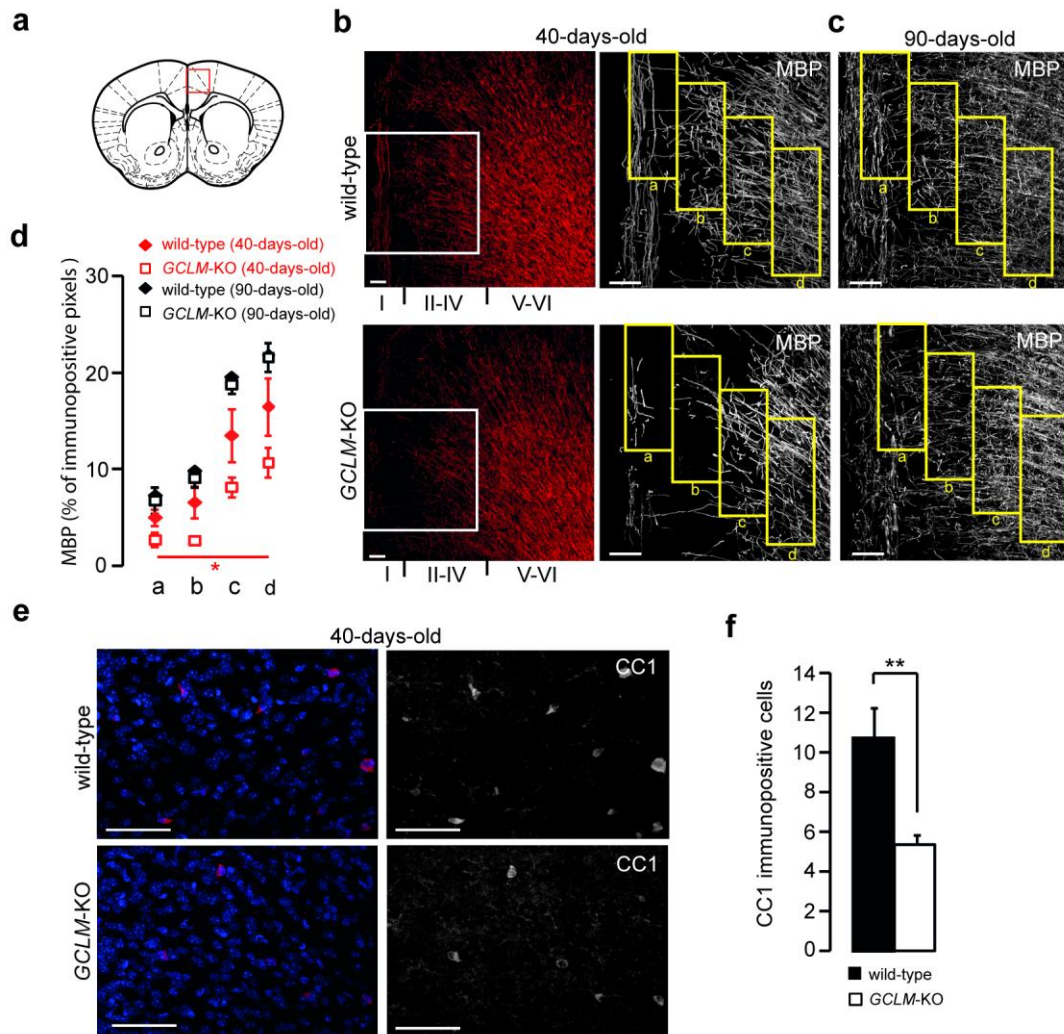


Figure 3

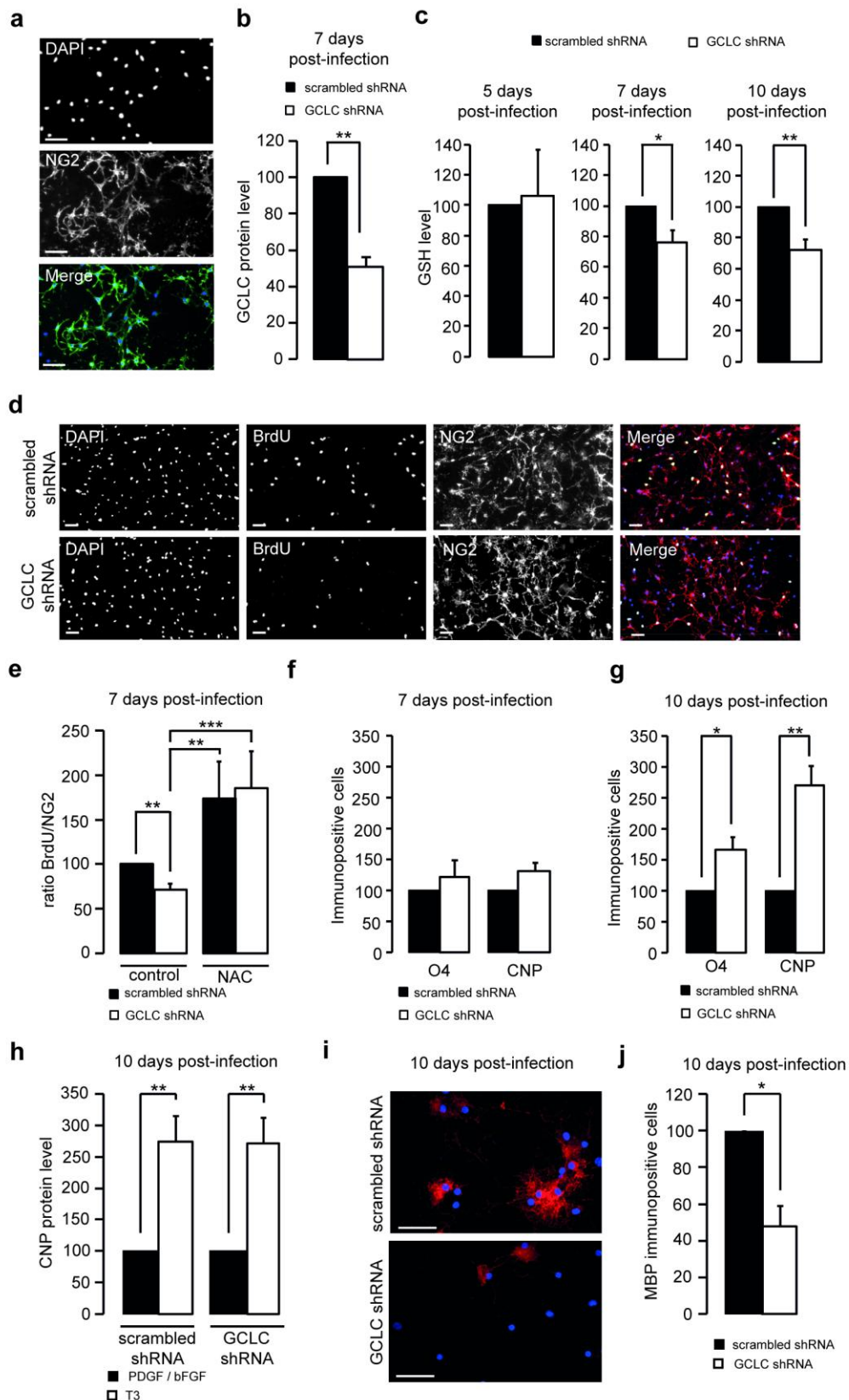
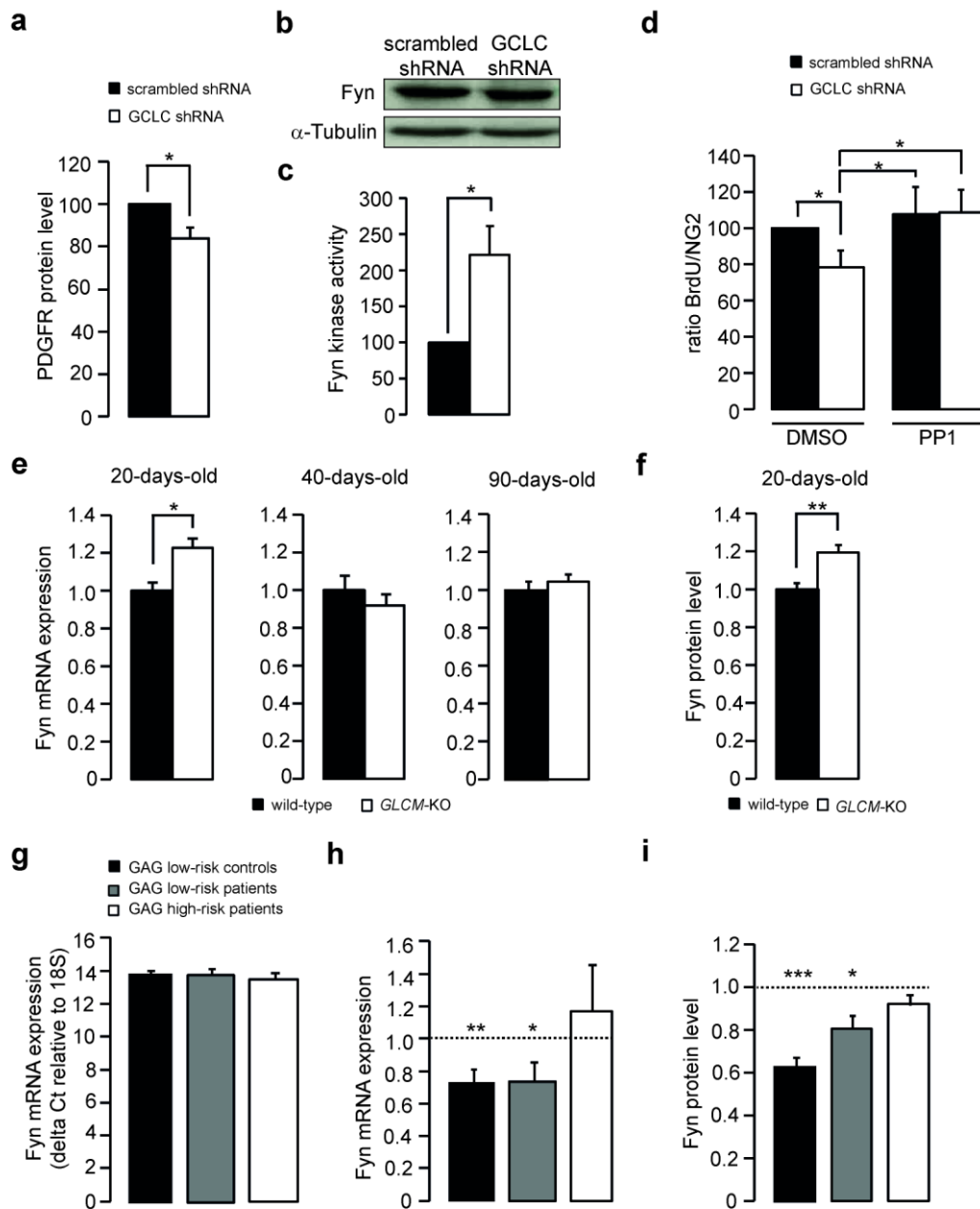
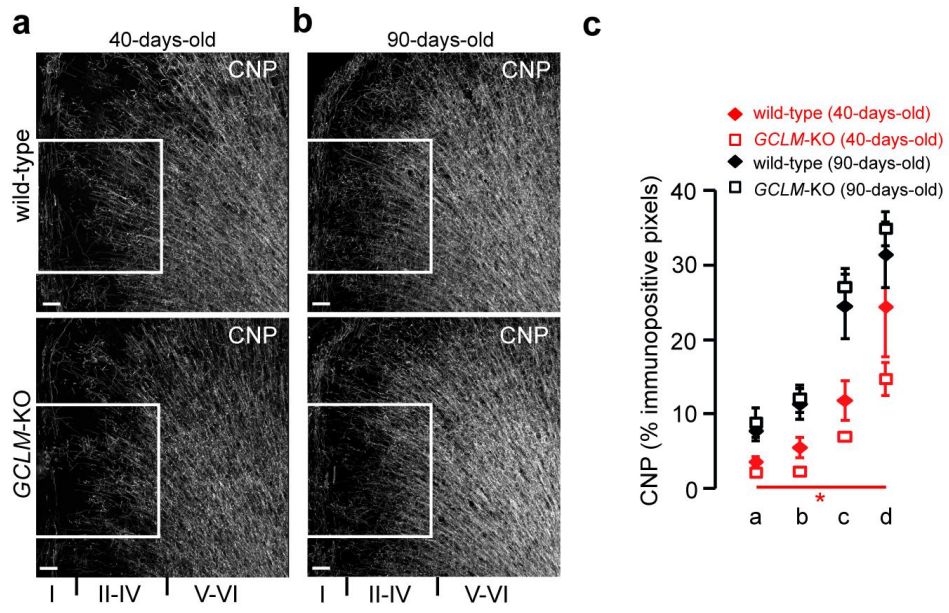


Figure 4

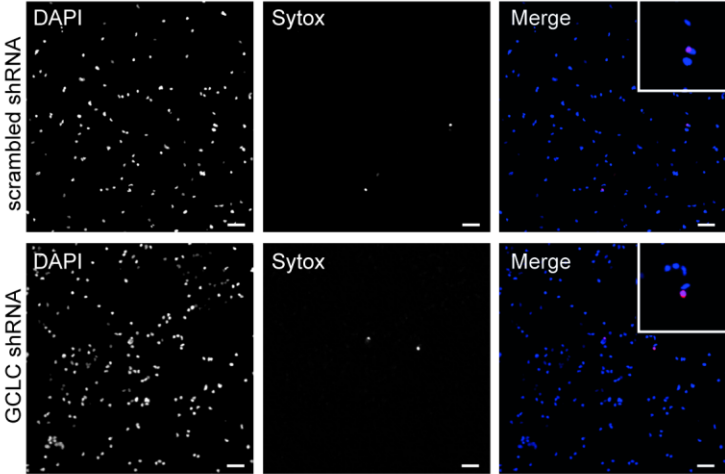


Supplementary Figure 1

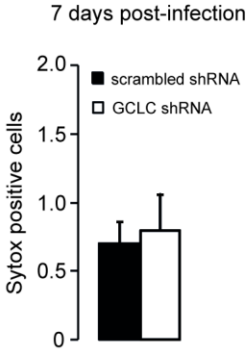


Supplementary Figure 2

a



b



Supplementary Figure 3

